

EXPERIMENTAL MEASUREMENT OF FLOW DISTRIBUTION IN A PARALLEL MINI-CHANNEL FLUIDIC NETWORK USING PIV TECHNIQUE

Boutin G., Biotteau G., Wei M., Fan Y., Luo L.,* and Lefevre N.

*Author for correspondence

Laboratoire de Thermocinétique de Nantes, UMR CNRS 6607, Polytech' Nantes – Université de Nantes
Nantes, 44306,

France,

E-mail: lingai.luo@univ-nantes.fr

ABSTRACT

Fluid flow distribution among parallel channels usually play an important role on the global performance improvement of tubular process equipment, but remains difficult to be properly measured by experimental methods. This paper presents a systematic study on the measurement of flow distribution in a multi-channels fluidic network using PIV technique. For the precise measurement of flow-rate in each individual channel, standard 2D-2C PIV technique is used to obtain velocity vectors on multiple sampling planes parallel to the flow direction, so as to reconstruct accurate velocity profiles on the cross-sectional surface. Such procedure is repeated for every channel to obtain the actual flow distribution properties in the fluidic network.

Pre-test results on a double-channels device indicate that the maximum possible deviation of PIV measurements is 13.1% with respect to those of a flange flowmeter, implying that the PIV technique is relatively accurate and reliable. PIV results on the flow distribution in a 15-channels fluidic network are then compared with CFD simulation results under the same working conditions. A quite good agreement could be observed. Moreover, the locations and sizes of vortices in the distributor have a significant influence on the flow distribution.

INTRODUCTION

Multi-channel micro- or mini-fluidic equipment usually consists of one inlet distributor, a number of parallel micro- or mini-channels and one outlet collector. They are widely used in process engineering and energy conversion systems, such as heat exchangers, chemical reactors, catalytic monoliths or fuel cells [1]. The fluid flow distribution among the parallel channels may play an important role on the achievement or improvement of their global performance [2-4]. Therefore, the precise measurement of mass (volume) flow-rate in each individual channel and then the flow distribution properties among parallel channels are an essential step for the diagnostic and improvement of flow distribution quality.

Recently, Particle Image Velocimetry (PIV) technique has undergone a rapid development which benefits from the advances in laser and camera technologies. Abundant studies in the literature have been devoted to the improvement of PIV technique for flow field measurement. However, most of these studies were focused on single channel [5-9], or at best on two parallel channels [10]. To the best of our knowledge, systematic

and precise measurement of flow distribution among multiple micro- (mini-) channels using PIV technique is still lacking.

As a result, the present study aims at realizing PIV measurement of the flow-rates in parallel channels and studying the fluid flow distribution in a multiple channels fluidic network. Firstly for the precise measurement of flow-rate in a single channel, standard PIV technique will be used to obtain the 2D-2C (2 dimensions, 2 components) velocity vectors on multiple planes parallel to the flow direction, so as to reconstruct accurate velocity profiles on the cross-sectional surface taking the potential effects of boundary layers into account. Secondly, such procedure will be repeated for every micro- (mini-) channel in the fluidic network so as to obtain the actual flow distribution properties among parallel channels.

In the rest of this paper, we shall first introduce the experimental set-up and the PIV instruments used in this study. The measurement parameters, the experimental procedure and the uncertainty will be discussed using a double-channels device as an example. Then, a mini-fluidic network having 15 parallel channels will be tested under different total inlet flow-rate conditions. The flow-rate distribution among parallel channels obtained by PIV technique will be compared with CFD simulation results under the same operational conditions.

EXPERIMENTAL SET-UP AND PIV INSTRUMENTS

Figure 1 shows the schematic diagram of the experimental set-up built in the laboratory LTN in Nantes, France. It consists of fluid circuit and PIV measurement facility. The working fluid used in this study was pure water. In the fluid circuit, water was pumped from a 300 L water tank, then passed through the test section (mini-channels device), and finally returned back to the water tank to form a closed loop. Due to the wide range of tested flow-rate conditions, two pumps were installed in the test-rig: a gear pump (MICROPUMP, O/CGC-M35.PVSF) with a measurement range of 1-5 L·min⁻¹ and a precise pump (VWR, REGLO-Z) with a measurement range of 32-3200 mL·min⁻¹. A tee joint was installed in the fluid circuit for the alternation of different pumps. The output flow-rate can be measured by a flange flowmeter (KOBOLD, DPL-1P15GL443, 0.2-6 L·min⁻¹) with ±2.5% instrumental error of the full scale (e.g., 0.15 L·min⁻¹) when the gear pump was used. For the precise pump, the flow-rate can be obtained by its own readings.

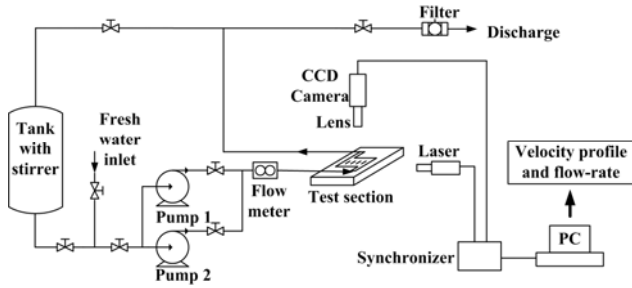


Figure 1 Schematic diagram of experimental setup

Standard 2D-2C PIV facility was used in our study. It consists of illumination unit, image record unit, synchronous controlling unit and data processing unit. The light source used was Nd-Yag laser (Litron Incorporation, DualPower 65-15 DANTEC laser) with a second harmonic generator which can produce a Q-switched output. The pulse energy was 65 mJ with the duration of 4 ns. The light wavelength was 532 nm and the diameter of light beam was 6.5 mm. The pulse frequency equalled to 5Hz, indicating that the fluid flow was recorded five times per second. The optical head was also a part of illumination unit which was installed at the end of laser guide. Consisting of spherical and cylindrical lenses, the pulse laser beam was converted into a pulse light sheet. The position (600 mm in this study) and the thickness of the light sheet can be adjusted by a commercial optical unit (DANTEC, 80×63).

The light scattered from the particles was collected by a CCD camera (DANTEC, FlowSense) with 2048×2048 pixels. The minimum time interval between two frames was 1 μ s. An additional macro LAVISION lens was used to yield a magnification of about 260 pixel·mm⁻¹ for double-channels device and about 230 pixel·mm⁻¹ for 15-channels device. Therefore, the view field was 7.87×7.87 mm and 8.73×8.73 mm, respectively. A synchronizer (DANTEC, 80N77) was used to guarantee that the laser and the CCD camera work synchronously. Commercial software FlowManager (v3.41) was used to control the PIV system and to process the data by 2-frame cross-correlation and Fast Fourier Transforms (FFTs). After that, the velocity vector profiles could be obtained. In the current study, the size of the PIV interrogation window was fixed at 16×16 pixels with an overlap of 50% after several attempts considering a compromise between the measurement accuracy and the computational time. The spatial resolution of PIV is determined by 2.8 times of the size of interrogation window [11]. Therefore, the physical spatial resolution was 0.17 mm for double-channels device and 0.19 mm for 15-channels device.

A workbench which permits the subtle movements of the test-section was specially designed and built. The camera may be moved in *x* direction whereas the platform to fix the test-section is moveable in *y* and *z* directions, as shown in Fig. 2. The movements in *x* and *y* directions were realized using steel orbits while the movement of the platform along *z* direction was realized using a precise lift and a digital gauge with an accuracy of 0.01 mm. Due to the different scattered light optical paths, the focus of the lens must be adjusted for each vertical plane, leading to different magnification ratios which

must be taken into account in the post-processing. It should be noted that the platform can also be rotated around *z*-axis to ensure a fine overlap between the walls of channels and the boundaries of the PIV interrogation window.

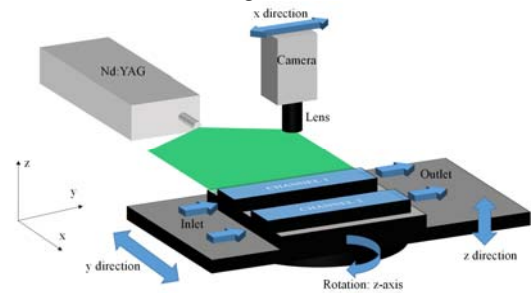


Figure 2 Schematic view of the experimental workbench for subtle movements of the test-section

Polyamid Seeding Particles (PSP-5) supplied by DANTEC Company were used as seeding in our study with good chemical stability and environmental friendliness. The particle density is 1030 kg·m⁻³ and the diameter of particles ranges from 1 μ m to 10 μ m with the average of 5 μ m. The Stokes number of PSP-5 is less than 1, indicating that the particles follow the flow streamlines well. A stirrer was employed in the water tank to ensure a homogeneous spatial distribution of the seeding particles in the working fluid flow.

MEASURING PROCEDURE AND PRE-TEST RESULTS

A double-channels device was fabricated using Polymethyl Methacrylate (PMMA) material, as shown in Fig. 3, for the purpose of confirming the feasibility of the 2D-2C PIV technique for parallel channels under multiple refractions. Each channel has a square cross-section of 5 mm×5 mm. The total channel length is 320 mm (the transparent part being 100 mm), longer than 20 times of its hydraulic diameter to ensure the fully-developed flow [12]. The distance between the axes of two channels is 15 mm. The channel closer to the laser source is named as CH1 while the other one is named as CH2. A static pressure probe and a valve were installed at the inlet of each channel to adjust the balanced flow-rates needed in the following test.

We define the middle plane of channels parallel to the flow direction as the base plane (*z*=0) so that the cross-section of channels ranges from *z*=-2.5 mm to *z*=+2.5 mm. In order to construct accurate fluid flow field, the cross-section of channels was divided into 21 planes along *z* axis, with a stepping distance of 0.25 mm to be measured.

For each measuring plane, a large number of frames (200 or 375 pairs in this study) should be captured and averaged to eliminate the random errors. Likewise, different planes were measured successively to obtain the fluid flow velocity vectors in *y*-*z* plane. Note that for each plane, the acquisition parameters (e.g., the focus of the lens, the time interval between two laser pulses, and the laser energy) should be adjusted according to different vertical positions, implying different magnifications of lens. In the post-processing, different relationships between the actual length (the width of channel in

this study) and the corresponding numbers of pixels should be used by introducing a magnification ratio G defined as follows:

$$G = N/l \quad (1)$$

where l is the width of the channel and N is the corresponding pixel numbers in the captured image. Due to non-identical values of G for different measured planes, the actual velocity U should be recalculated as follows:

$$U = U'/(G\Delta t) \quad (2)$$

where U' is the flow velocity obtained by PIV post-processing under the unit of pixels/frame and Δt is the time interval between two frames. A MATLAB programme was built to handle the calculation process automatically.

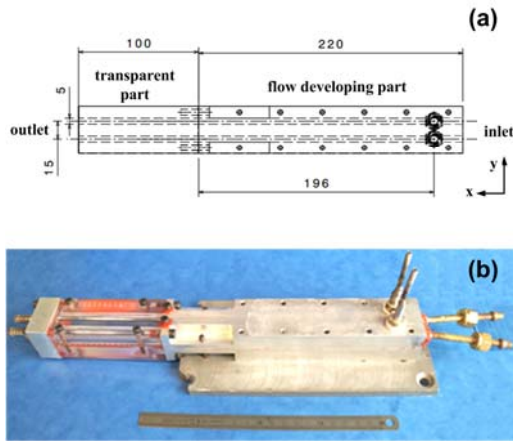


Figure 3 The geometry and dimensions of double-channels device: (a) schematic view (unit: mm); (b) photo view

Once the unit conversions for all measuring planes were finished, a fixed physical position (for example the middle of the image) for all measuring planes was chosen as the transverse surface and the fluid flow velocity profiles at y - z surface could be obtained, as an example shown in Fig. 4. The boundary layers near the side walls could be clearly observed.

Based on the fluid flow velocity profiles at y - z surface (cross-section), the mass flow-rate m passing through the channel can be easily obtained as follows:

$$m = \rho Q = \rho \int_S U dS \quad (3)$$

where Q is the volume flow-rate, S is the area of the cross-section of the channel and ρ is the density of water used in our study ($998.2 \text{ kg}\cdot\text{m}^{-3}$). The channel Reynolds number is calculated as:

$$\text{Re} = d_h \bar{U} \rho / \mu \quad (4)$$

where \bar{U} is the mean fluid velocity in a channel, μ the dynamic viscosity of water and d_h the hydraulic diameter of the channel calculated as:

$$d_h = 4S / A \quad (5)$$

where A is the perimeter of the channel's cross-section.

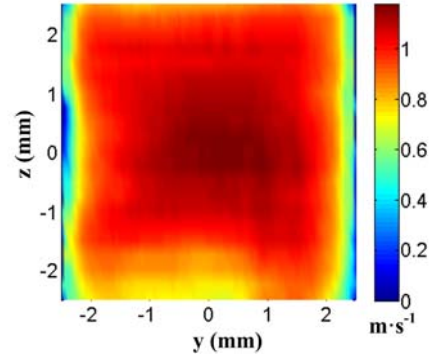


Figure 4 Example of fluid flow velocity profile at the cross-sectional surface of a channel

It should be noted that due to the limitation of the test view of PIV, at most two channels can be measured together each time. For the 15-channels device with 2 mm in depth, eight successive measurements (thus 72 planes) should be processed to obtain the fluid flow distribution properties among parallel channels.

In order to analyze the uncertainty of the 2D-2C PIV technique, three cases of pre-test were carried out. In Case 1, the fluid flow just passed through CH1 as a standard PIV measurement in single channel. In Case 2, the fluid flow was injected through CH2 while CH1 was filled with still water to simulate a parallel channel configuration, so that the laser sheet had to pass through CH1 firstly before reaching CH2. In Case 3, the volume flow-rates in both channels were measured simultaneously, with balanced flow-rates adjusted according to the static pressure probes. The results obtained by PIV (Q_p) were compared with the measurements of the flowmeter (Q_f), as listed in Table 1. Recall that the flowmeter has a $\pm 2.5\%$ maximum instrumental uncertainty. Therefore, The minimum and maximum deviations of the PIV measurements are defined as follows:

$$\varepsilon_{\min/\max} = \left| \frac{Q_p - (Q_f \pm 0.15)}{Q_f \pm 0.15} \right| \quad (6)$$

Table 1 The results of different cases in pre-test

No. Case	Frame number for each plane	Q_f (L·min ⁻¹)	Q_p (L·min ⁻¹)	ε_{\min} (-)	ε_{\max} (-)
Case 1	200	1.470	1.4081	6.67%	13.1%
(CH1)	375	1.470	1.4096	6.79%	13.0%
Case 2	200	1.450	1.4170	9.00%	11.4%
(CH2)	375	1.450	1.4174	9.03%	11.4%
Case 3			1.5275		
(CH1+CH2)	200	3.085	(CH1)=1.4714 (CH2)=2.9989	2.18%	7.30%

Two numbers of instantaneous frames, 200 and 375, were used to test the image independence in Cases 1 and 2. It can be seen that the maximum deviation is less than 0.1%. Therefore, 200 pairs of frames for each plane were enough for the rest of the experiments. It can also be seen that the results obtained by PIV show a good agreement with the values of flowmeter. The

maximum possible deviation is 13.1% (will be indicated as the error bars for PIV results in the following figures), implying that the PIV technique is relatively accurate and reliable for flow-rate measurement.

MEASUREMENT OF FLOW-RATE DISTRIBUTION IN A MULTI-CHANNEL FLUIDIC NETWORK

After the pre-test and uncertainty analysis of the 2D-2C PIV technique using the double-channels device, a 15-channels device with integrated distributor and collector was fabricated and tested to show the effectiveness and the validity of the experimental method, as shown in Fig. 5.

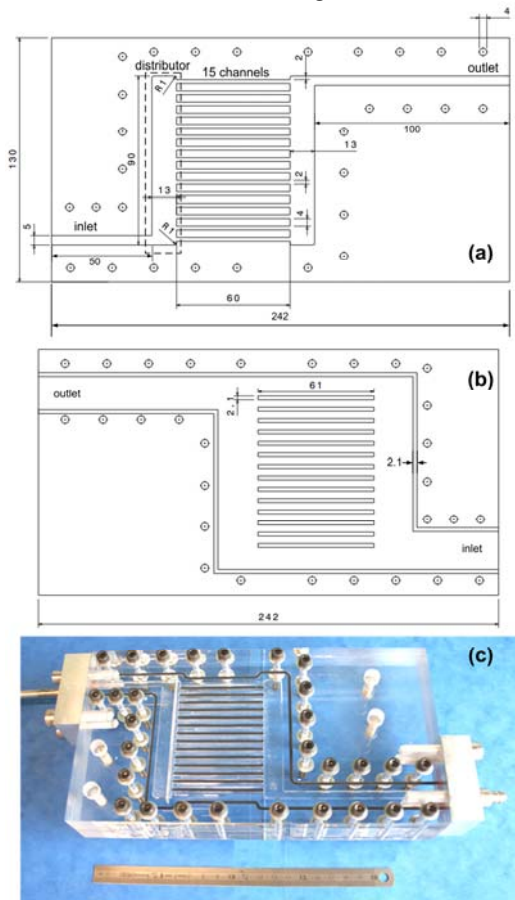


Figure 5 The geometry and dimensions of 15-channels fluidic network. (a) Cube A; (b) Cube B (unit: mm); (c) Photo view after assembling

The overall dimension is 242 mm in length and 90 mm in width. For the convenience of fabrication, the entire fluidic network has the identical channel depth ($e=2$ mm). The inlet and outlet channels located in diagonal position have the same width of 5 mm, but different lengths (50 mm for inlet tube and 100 mm for outlet tube). The length of the distributing manifold is 13 mm and the width is 90 mm. Identical dimensions are used for the collecting manifold (length of 13 mm and width of 90 mm). There are fifteen parallel straight channels with identical width of 2 mm, length of 60 mm and depth of 2 mm. They are evenly spaced at 4 mm between the axis of one

channel and another. For the convenience of description, they are indexed by k from 1 to M from the inlet side to the outlet side. By this way, the mass flow-rate in k th channel is notated as m_k . The flow-rate ratio σ is introduced for each channel as follows:

$$\sigma_k = m_k / \bar{m} \quad (7)$$

where \bar{m} is the average mass flow-rate among 15 channels given by:

$$\bar{m} = \left(\sum_{k=1}^M m_k \right) / M \quad (8)$$

The device was also fabricated in the laboratory LTN by carving the network on the surface of a PMMA cube (cube A), as shown in Fig. 5a. Six edge fillets having the same radius of 1 mm may be observed at different corners of the fluidic. Another PMMA cube (cube B) was also carved to form the enclosed fluidic network, as shown in Fig. 5b. To prevent the water leakage, a number of grooves were reserved around the network or between the parallel channels, and filled with rubble strips. The photo view of the 15-channels device after assembling may be found in Fig. 5c.

CFD SIMULATION

3D CFD simulation was also performed to calculate the flow-rate distribution among 15 parallel channels and to compare with the PIV measurements. The geometrical characteristics used in the simulation were exactly the same as the fabricated device, including the edge fillets. The working fluid used was pure water at ambient temperature with density of $998.2 \text{ kg}\cdot\text{m}^{-3}$ and viscosity of $1.003 \times 10^{-3} \text{ kg}\cdot\text{m}^{-1}\cdot\text{s}^{-1}$. The inlet mass flow-rate was set to be constant according to different operation conditions. The operational pressure was fixed at 101325 Pa. Simulations were performed under steady state, incompressible and isothermal condition without heat transfer. The gravity effect at $-z$ direction was also taken into account.

A commercial code FLUENT (version 12.1.4) was used to solve the Navier-Stokes equations. The fluid flow was calculated by the COUPLED method for pressure-velocity coupling, and second-order upwind differential scheme was applied for discretization of momentum and standard method for pressure. Laminar or standard $k-\epsilon$ model was used to simulate the laminar or turbulent flow, respectively. Constant mass flow-rate at inlet surface was given and the boundary condition of outlet was set as pressure-outlet with zero static pressure. Adiabatic wall condition was applied and no slip occurred at the wall. The solution was considered to be converged when 1) sums of the normalized residuals for control equations were all less than 1×10^{-6} ; and 2) the mass flow-rate at each channel was constant from one iteration to the next (less than 0.5% variation).

The grid density used in the study was 5 segments per millimeter (1.42 million elements in total) and structured mesh was generated using software ICEM (version 12.1) to build up the geometry model. A grid independence study was performed

with a refined mesh (8 segments per millimeter; 5.49 million elements in total). Simulation results with the inlet volume flow-rate of $1.8 \text{ L}\cdot\text{min}^{-1}$ indicated a difference of about 3.2% on the inlet pressure. For the mass flow-rate in each channel, the maximum difference was less than 4.9%. Therefore, the normal mesh was used as a compromise between the calculation time and the precision while the value of 4.9% was indicated as error bars for the CFD results in the following figures.

RESULTS AND DISCUSSIONS

Two different inlet total fluid flow-rates (Q_{in}) were tested in this study, i.e. high inlet flow-rate of $1.8 \text{ L}\cdot\text{min}^{-1}$ and low inlet flow-rate of $0.18 \text{ L}\cdot\text{min}^{-1}$, in order to cover both the laminar and the turbulent flow patterns. The corresponding Re number at the inlet channel (Re_{in}) was 8500 and 850, respectively. The mean Re number in the parallel channels (Re_{ch}) was 1000 for $Q_{in}=1.8 \text{ L}\cdot\text{min}^{-1}$ and 100 for $Q_{in}=0.18 \text{ L}\cdot\text{min}^{-1}$. The numerical (CFD) and experimental (PIV) results on fluid flow distribution among the 15 parallel channels are shown in Fig. 6.

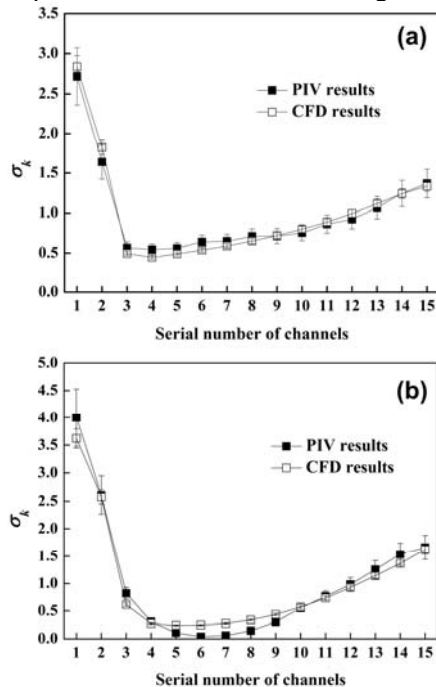


Figure 6 The flow distribution properties obtained by PIV and CFD under different inlet flow-rate conditions. (a) $Q_{in}=0.18 \text{ L}\cdot\text{min}^{-1}$, mean $Re_{ch}=100$; (b) $Q_{in}=1.8 \text{ L}\cdot\text{min}^{-1}$, mean $Re_{ch}=1000$

Under low inlet flow-rate condition ($Q_{in}=0.18 \text{ L}\cdot\text{min}^{-1}$; mean $Re_{ch}=100$), the flow distribution curve appears a V-like shape, as shown in Fig. 6a. The values of flow-rate are relatively high ($\sigma_k > 1.5$) in channels facing to the inlet tube (e.g. channels 1 and 2) and then decrease rapidly to the lowest in channel 4. After that, a slow increase of flow-rate appears till the channel 15 which is the farthest channel from the inlet tube. The flow distribution is obviously non-uniform, with the σ_k values ranging from 0.55 to 2.72 (PIV results). It can also be observed that the CFD and PIV results are in good agreement, implying that the laminar model is capable of correctly simulating the fluid flow under low flow-rate condition.

CFD and PIV results on flow distribution under high inlet flow-rate condition ($Q_{in}=1.8 \text{ L}\cdot\text{min}^{-1}$; mean $Re_{ch}=1000$) are shown in Fig. 6b. A similar but less uniform distribution curve (U-like shape) may be observed compared to that under low-rate condition, with σ_k values ranging from 0.04 to 4.00 (PIV results). It may be observed that the CFD results are in good agreement with the PIV results for the general tendency. However, noticeable discrepancies may also be observed especially for channels 5-9, implying the potential difficulties in simulation caused by turbulence and vortex flows.

In order to better validate the CFD simulations by PIV measurement, a detailed examination on the fluid flow streamlines in the distributor was carried out. Due to the limitation of view field, the inlet distributor section was divided into seven independent parts which were successively recorded by the CCD camera when the fluid flow was stable, each part having 200 instantaneous frames for the PIV post-treatment. These parts were then processed and connected so as to reconstruct the fluid flow streamlines in the whole distributor section, except for a narrow bar area which is not transparent due to fabrication limitation. Results under low and high inlet flow-rate conditions are presented in Fig. 7 and Fig. 8, respectively. Corresponding flow streamlines obtained by CFD simulation under the same working conditions are also included for comparison.

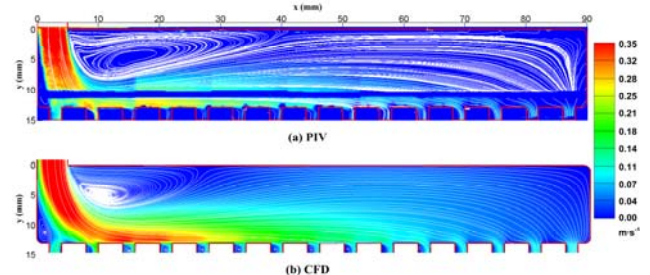


Figure 7 The streamlines in the distributor section under low inlet flow-rate condition ($Q_{in}=0.18 \text{ L}\cdot\text{min}^{-1}$, mean $Re_{ch}=100$). (a) PIV measurement; (b) CFD simulation

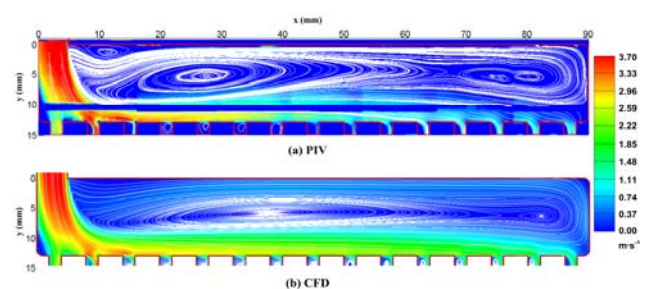


Figure 8 The streamlines in the distributor section under high inlet flow-rate condition ($Q_{in}=1.8 \text{ L}\cdot\text{min}^{-1}$, mean $Re_{ch}=1000$). (a) PIV measurement; (b) CFD simulation

Under low inlet flow-rate condition ($Q_{in}=0.18 \text{ L}\cdot\text{min}^{-1}$; mean $Re_{ch}=100$), both the flow streamlines in the distributor section obtained by PIV and CFD methods seem smooth and regular. Because of the small opening of parallel channel with respect to the inlet tube, a part of fluid flow changes the direction by 90° , passing horizontally towards the edge wall of

the distributor. Some inlets located in the middle of the network (e.g., channels 3-11) are partially skipped by the fluid flow, indicated by the σ_k values smaller than 1.0. Owing to the back-flow from the edge wall (boundary effect), the farthest channels (e.g., channels 14-15) receive relatively higher amount of fluid flow than the average ($\sigma_k > 1.0$). A vortex next to the inlet tube may be easily observed both on PIV and CFD images, with similar location and size. This also explains the good agreement between PIV and CFD results on flow-rate distribution among parallel channels.

Under high inlet flow-rate condition ($Q_{in}=1.8 \text{ L}\cdot\text{min}^{-1}$; mean $Re_{ch}=1000$) however, the flow profiles in the distributor chamber become irregular, indicated by the existence of more and larger vortices and recirculation flows. The images of flow streamlines obtained by PIV and CFD methods appear to be globally similar but slight different in detail, especially on the size of vortices in y direction. This implies that the locations and sizes of vortices in the distributor section are the key factors influencing the flow distribution properties among parallel channels.

CONCLUSIONS AND PERSPECTIVES

In this work, the fluid flow distribution properties in a parallel mini-channels fluidic network have been measured using PIV technique. The standard 2D-2C PIV has been employed to measure the mass flow-rates by dividing the cross-sections of channels into a number of sampling planes. The flow-rates obtained by PIV technique have been compared with the values of flowmeter for a double-channels device and with CFD simulation results for a 15-channels fluidic network. Based on the analyses presented above, the following conclusions may be reached:

- PIV technique provides the advantages of whole field and non-intrusive measurement. It is a relatively accurate and reliable experimental method for flow-rate measurement, with the maximum possible uncertainty of 13.1% under our tested conditions.
- Non-uniform flow distributions among multiple parallel channels are observed by both PIV and CFD methods. Under low flow-rate ($Q_{in}=0.18 \text{ L}\cdot\text{min}^{-1}$; mean $Re_{ch}=100$), CFD results show excellent agreement with the PIV measurements. Under high flow-rate ($Q_{in}=1.8 \text{ L}\cdot\text{min}^{-1}$; mean $Re_{ch}=1000$), the numerical and experimental results are in good agreement for the general tendency, but noticeable discrepancies on the flow-rate in certain channels may also be observed.
- A close investigation on the flow streamlines in the distributor section indicates that the measurement discrepancies under high flow-rate condition are mainly due to the difficulties in simulation caused by turbulence and vortex flows. Actually the locations and sizes of vortices in the distributor may have a significant influence on the flow distribution. This also implies that CFD results must be validated by experimental measurements, especially under turbulent flow condition.

Once the reliable technique has been established for the precise measurement of flow distribution, the next task is how to control the flow distribution properties so as to improve the global performances of tubular process equipment or energy conversion systems. In some cases, a uniform distribution

among parallel channels is generally required, while in many other cases, a target flow distribution which is non-uniform should be achieved [13]. In our earlier work, an original CFD-based evolutionary algorithm has been proposed to realize uniform or non-uniform fluid flow distribution among parallel channels [14,15]. The experimental validation of this optimization method with the PIV technique developed in this paper is our on-going work.

REFERENCES

- [1] Luo L., Heat and Mass Transfer Intensification and Shape Optimization: A Multi-scale Approach. Springer, London, 2013.
- [2] Lalot S., Florent P., Lang S., and Bergles A., Flow maldistribution in heat exchangers. *Applied Thermal Engineering*, Vol. 19(8), 1999, pp. 847-863.
- [3] Luo L., Fan Y., and Tondeur D., Heat exchanger: From micro- to multi-scale design optimization. *International Journal of Energy research*, Vol. 31, 2007, pp. 1266-1274.
- [4] Fan Y., Boichot R., Goldin T., and Luo L., Flow distribution property of the constructal distributor and heat transfer intensification in a mini heat exchanger. *AIChE Journal*, Vol. 54(11), 2008, pp. 2796-2808.
- [5] Meinhardt C.D., Wereley S.T., and Santiago J.G., PIV measurements of a microchannel flow. *Experiments in Fluids*, Vol. 27, 1999, pp. 414-419.
- [6] Kitagawa A., Hishida K., and Kodama Y., Flow structure of microbubble-laden turbulent channel flow measured by PIV combined with the shadow image technique. *Experiments in Fluids*, Vol. 38, 2005, pp. 466-475.
- [7] Hoffmann M., Schlüter M., and Rübiger N., Experimental investigation of liquid-liquid mixing in T-shaped micro-mixers using μ -LIF and μ -PIV. *Chemical Engineering Science*, Vol. 61, 2006, pp. 2968-2976.
- [8] Lima R., Wada S., Tsubota K., and Yamaguchi T., Confocal micro-PIV measurements of three-dimensional profiles of cell suspension flow in a square microchannel. *Measurement Science and Technology*, Vol. 17, 2006, pp. 797-808.
- [9] Silva G., Leal N., and Semiao V., Micro-PIV and CFD characterization of flows in a microchannels: Velocity profiles, surface roughness and Poiseuille numbers. *International Journal of Heat and Fluid Flow*, Vol. 29, 2008, pp. 1211-1220.
- [10] Shinohara K, Sugii Y, Aota A, Hibara A, Tokeshi M, Kitamori T, and Okamoto K. High-speed micro-PIV measurements of transient flow in microfluidic devices. *Meas. Sci. Technol.* 2004; 15: 1965-1970.
- [11] Foucaut J.M., Carlier J., and Stanislas M., PIV optimization for the study of turbulent flow using spectral analysis. *Measurement Science and Technology*, Vol. 8, 2004, pp. 1427-1440.
- [12] Hinze J.O., Turbulence. McGraw Hill Company, 1959.
- [13] Wei M., Fan Y., Luo L., and Flamant G., Fluid flow distribution optimization for minimizing the peak temperature of a tubular solar receiver. *Energy*, Vol. 91, 2015, pp. 663-677.
- [14] Luo L., Wei M., Fan Y., and Flamant G., Heuristic shape optimization of baffled fluid distributor for uniform flow distribution. *Chemical Engineering Science*, Vol. 123, 2015, pp. 542-556.
- [15] Wei M., Fan Y., Luo L., and Flamant G., CFD-based evolutionary algorithm for the realization of target fluid flow distribution among parallel channels. *Chemical Engineering Research and Design*, Vol. 100, 2015, pp: 341-352.